Photoisomerization Dynamics of trans-trans, cis-trans and cis-cis Diphenylbutadiene from Broadband Transient Absorption Spectroscopy and Calculations

O. A. Krohn,² M. Quick,¹ S. M. Sudarkova,³ I. N. Ioffe,³* C. Richter,¹ S. A. Kovalenko¹*

¹ Department of Chemistry, Humboldt-Universität zu Berlin, Germany

² Departments of Physics and Chemistry, University of Colorado, Boulder, United States

³ Department of Chemistry, Lomonosov Moscow State University, Russia

Abstract

The photoisomerization path and dynamics of trans-trans (ttD), cis-trans (ctD) and cis-cis (ccD) 1,4-diphenyl-1,3-butadiene (DPB) in solution is studied with broadband transient absorption (TA) spectroscopy and quantum chemical calculations. With ttD, 2-photon excited TA spectra provide evidence that the $2A_g$ state is located higher than 1-photon allowed $1B_u(S_1)$ by ~ 1200 cm⁻¹, different from earlier estimates. Following $S_0 \rightarrow S_1$ optical excitation, the isomerization occurs via torsion about a butadiene double bond to perpendicular molecular configuration P. The P-state is detected in ccD with an excited state absorption (ESA) band at 390 nm. This P-band develops during $S_1 \rightarrow P$ half-torsion with time of 0.15 ps, followed by $P \rightarrow S_0$ further half-torsion and simultaneous decay with 1.6 ps in acetonitrile, and 5 ps in n-hexane. In addition, two cycles of population oscillations between P and S_1 before equilibration is observed in n-hexane. For ctD, an indication of rising and decaying P is found in acetonitrile. The vast majority of ctD species photoisomerizes to ttD, and not to ccD, in agreement with calculated low torsional barrier about the cis double bond, and high barrier about the trans double bond. Photoisomerization yield Y and time τ_1 depend drastically on

the solvent polarity. Thus in n-hexane, the isomerization ttD \rightarrow ctD has yield Y_{tt,ct}=0.1 and time τ_i =829 ps, while in acetonitrile Y_{tt,ct}=0.4 and τ_i =27 ps. The 30-fold acceleration of the isomerization in acetonitrile clearly reflects a highly polar character of *P* consistent with a dipole moment μ_P >9.6 D. The results for DPB are discussed in comparison to stilbene.

I. Introduction

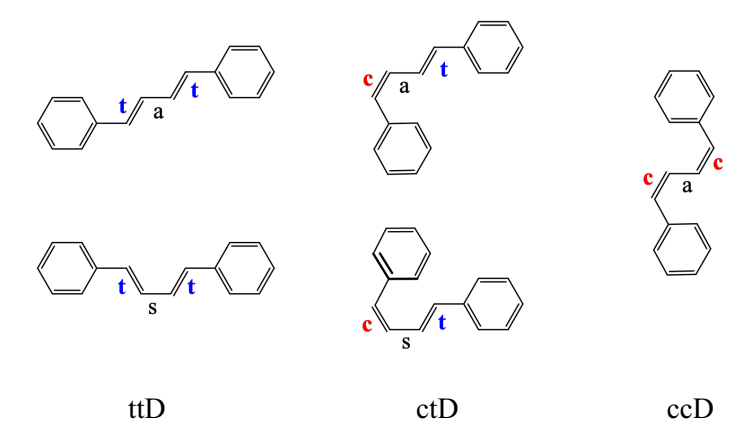
The photophysics and photochemistry of trans-trans-1,4-diphenyl-1,3-butadiene (ttDPB, or hereafter ttD) has been carefully studied in the past.¹⁻¹⁶ A major challenge was thoroughly testing Rice-Ramsperger-Kassel-Marcus (RRKM)^{17,18,9} and Kramers¹⁹⁻²¹ theory of unimolecular reactions, by comparing theoretical and experimental photoisomerization rates of ttD⁴⁻⁸ and of trans-stilbene (tSt)^{22-26,28-32} in gases (jets)^{9-12,17,18,27} and in liquids.^{4-8,22-26,28-32}

Another significant question consisted of the ordering of excited electronic states 2^1A_g and 1^1B_u in α, ω -diphenylpolyenes. For trans-stilbene it was established that 1-photon allowed 1^1B_u lays below optically forbidden 2^1A_g , both for the isolated and solvated molecule. However for ttD this is different: in solution the 1^1B_u state is located below $2^1A_g^{1.8}$ like in t-stilbene $^{26,28-32}$, but in vacuum the order is inverted and 1^1B_u appears to be higher than $2^1A_g^{1.8}$. An important consequence is that the photoisomerization dynamics of isolated ttD molecules in jets or low-pressure gases cannot be directly related to that in solution, since the photoisomerization proceeds from different electronic states. This contrasts the case of t-stilbene, where the photoisomerization starts from the same 1^1B_u state both in gases in liquids, and hence the corresponding rates can be directly compared. Here we do not address these interesting and important issues, but rather leaving them for a forthcoming article.

Until now, time-resolved spectroscopy of diphenylbutadiene was performed on ttD only, $^{3-8}$ not on cis-trans (ctD) or cis-cis (ccD) isomers. The present paper aims to fill this gap, and reports transient absorption spectra and kinetics of ctD and ccD in n-hexane and acetonitrile, as well as of ttD in a wider range of polar and nonpolar solvents. We further compare the experimental results to our quantum-chemical calculations for the isolated DPB molecule. We also apply 2-photon excitation of ttD, in order to estimate the origin of the $2A_g$ state in ttD and compare the DPB results to those of stilbene.

II. Quantum-Chemical Calculations

Quantum chemical calculations on DPB (the molecular structures are displayed in Scheme 1) are performed with the use of the Firefly QC package version 8.2^{33} which is partially based on GAMESS (US) source code and of the Gaussian oppackage. The ground state structures are optimized at the mPW2PLYP/Def2-TZVPP level of theory (Gaussian opposition) while the excited states are treated at the TD-PBE0/Def2-TZVPP level and with the use of the XMCQDPT2 multiconfiguration quasi-degenerate perturbation theory implemented in Firefly 8.2. The perturbation corrections are applied to the model space of the twelve CASSCF(12,12)/Def2-TZVPP singlet states obtained with averaging over the five lowest states in order to cover the essential contributions to S_1 and S_2 . Included in the active space are 12 of the total 16 π -orbitals of the molecule, with the exception of the lowermost and uppermost benzenoid π -orbitals. The XMCQDPT2 calculations are performed with frozen chemical core and an intruder state avoidance (ISA) shift of 0.02 a.u. All calculations are done without the use of symmetry.



Scheme 1. Possible cis- and trans-isomers of DPB with respect to the central double bonds and their *syn* (s) and *anti* (a) rotational isomers (rotamers) with respect to the central single bond (the unlikely cis-*syn*-cis is omitted).

III. Experiment

A. Compounds and Stationary Spectra

Stationary absorption spectra of the compounds under study are shown in Fig.1 Trans-trans DPB (ttD) (≤99%) was purchased from Fluka and measured without further purification. The ctD isomer was produced photochemically from ttD by illuminating an n-hexane solution of ttD with a mercury lamp in the range 275-375 nm (filter FGUV11, Thorlabs). About 0.4 g of ctD was collected, chromatographically purified (99%), and kept at -18°C. The ccD isomer was synthesized as described in Refs. 2, 3. Sample purity was checked by comparison with the extinction spectra of Fig. 1.

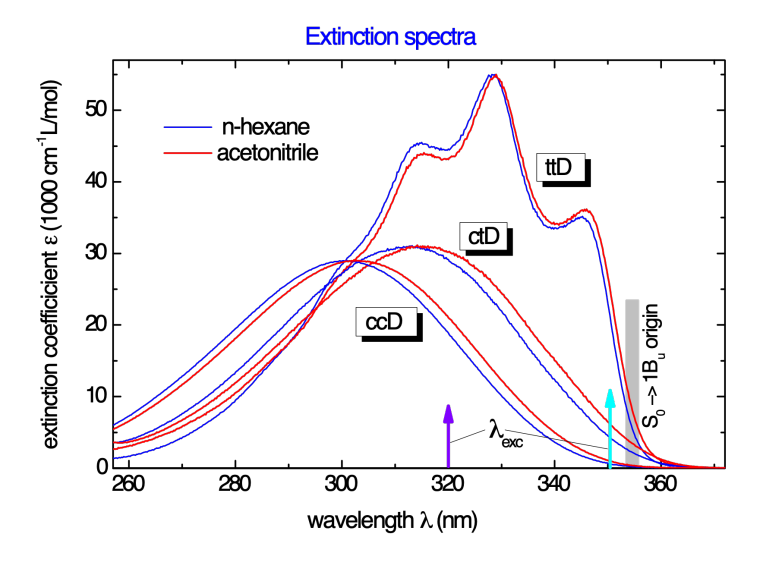


Fig. 1. Absorption spectra of trans-trans (ttD), cis-trans (ctD), and cis-cis (ccD) 1,4-diphenyl-1,3-butadiene in n-hexane and acetonitrile at 20°C. Optical excitation for TA is at 351 nm for ttD, and at 320 nm for ctD and ccD. The origin of the $S_0 \rightarrow S_1(1B_u)$ transition for ttD is taken to be at 354 nm indicated by grey bar.

B. Transient Absorption (TA)

Our TA setup with applications has been described elsewhere. TA spectra $\Delta A(\lambda,t)$ were recorded at the magic angle, and with parallel $\Delta A_{||}(\lambda,t)$ and perpendicular $\Delta A_{\perp}(\lambda,t)$ pump-probe polarization, in the spectral range 275-690 nm with 0.1 ps instrument response. Multiple (10-20) back-and-forth pump-probe scans were performed to improve the signal-to-noise ratio. Transient anisotropy is calculated as

$$\rho(\lambda, t) = (\Delta A_{\parallel} - \Delta A_{\perp})/(\Delta A_{\parallel} + 2\Delta A_{\perp}) = (\Delta A_{\parallel} - \Delta A_{\perp})/(3\Delta A) \tag{1}$$

The anisotropy decay time, or rotational diffusion time τ_R , was obtained from a monoexponential fit of $\rho(t)$.

A 30 ml solution with 0.4 mg/mL of ttD, or 1.2 mg/mL of ctD or ccD was flown through a sample cell of 0.3 mm internal thickness. The absorbance $A(\lambda)$ at the excitation wavelength was kept less than 0.6. The pump and probe beams intersect at 15° and were focused onto the cell to 0.2 mm diameter.

The ctD signal has a ttD contribution that should be subtracted. The amplitude of that contribution is found from the long-time behavior of the TA signal, when the ctD signal disappears and only the ttD one remains. Similarly, the ccD signal has ctD and ttD contributions subtracted in the same way.

A global analysis over the TA kinetics, fitted by a sum of exponentials, was applied to derive the decay constants and amplitudes. The joint sets of data with different time steps were analyzed to ensure the resulting fits match each other. Averaged kinetics are represented by band integrals:

$$I(\lambda_1, \lambda_2, t) = \frac{1}{\ln(\lambda_2/\lambda_1)} \int_{\lambda_1}^{\lambda_2} \Delta A(\lambda, t) d\lambda/\lambda \tag{2}$$

These integrals are calculated either directly from experimental spectra or from the corresponding global fits. When the spectral range (λ_1, λ_2) is carefully chosen, the band integrals $I(\lambda_1, \lambda_2)$ improve the signal-to-noise and eliminate the contribution from spectral shifts.

For ttD the photoisomerization time τ_i is calculated from the measured decay τ_d as,

$$1/\tau_{\rm i} = 1/\tau_{\rm d} - 1/\tau_{\rm rad} \tag{3}$$

with the radiative decay τ_{rad} =1.5 ns taken to be the same in all our solvents. Thus we neglect a weak dependence of τ_d on solvent due to excited-state mixing of $1B_u$ and $2A_g$. The photoisomerization yields Y are obtained from a global fit in the bleach region, λ < 360 nm, using early $\Delta A(\lambda,0)$ and late $\Delta A(\lambda,\infty)$ spectra. For example, for the tt—ct isomerization one gets

$$\Delta A(\lambda, \infty) = \Delta A(\lambda, 0) [1 - Y_{tt,tt} - Y_{tt,ct} \varepsilon_{ct}(\lambda) / \varepsilon_{tt}(\lambda)]$$
(4)

Here both Y_{tt,tt} and Y_{tt,ct} are varied to achieve the best fit.

IV. TA Spectra and Kinetics

A. ttDPB

TA spectra of ttD in n-hexane and acetonitrile upon $S_0 \rightarrow S_1$ excitation at 351 nm are shown in Fig. 2. Note that bleach and stimulated emission (SE) contribute a negative signal, while excited-state absorption (ESA) is positive, and arrows indicate the signal evolution. Early spectra -0.08 < t < 0.1 ps within the pump and probe overlap, are displayed on top. Fast Franck-Condon (FC) relaxation with $\tau < 1$ ps is seen in the second frames. Afterwards, the signal decays monoexponentially with $\tau_d = 534$ ps in n-hexane and $\tau_d = 26$ ps in acetonitrile, reflecting torsion $S_1 \rightarrow P$ from plane to perpendicular molecular configuration P. The monoexponential decay is consistent with the presence of one rotamer only, in agreement with our calculations. Also, the $P \rightarrow S_0$ transition is to be much faster than $S_1 \rightarrow P$, since no P-species are visible. The rotational diffusion time τ_R (or the anisotropy decay time, Eq. (1)) is found to be 24 and 33 ps in n-hexane and acetonitrile, respectively.

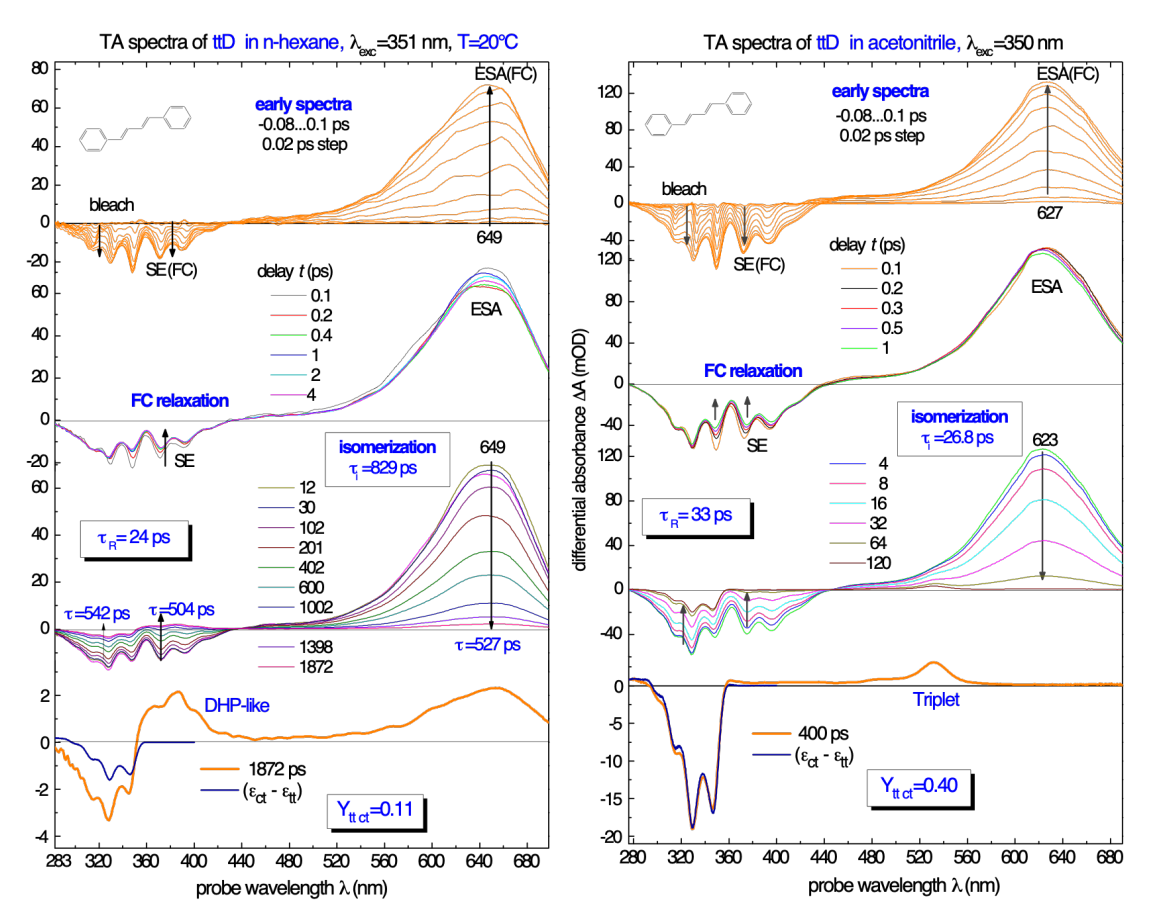


Fig. 2. Transient absorption (TA) spectra $\Delta A(\lambda,t)$ of ttD upon $S_0 \rightarrow S_1$ excitation. Bleach and stimulated emission (SE) are negative, excited-state absorption (ESA) is positive, arrows indicate the signal evolution. Early spectra at -0.08 < t < 0.08 ps are on top. The signal decays monoexponentially with $\tau_d = 534$ ps in n-hexane and 26 ps in acetonitrile, reflecting torsion $S_1 \rightarrow P$ to perpendicular conformation P. The decay of SE is shorter by 10% than that of bleach and ESA; a similar effect is observed for t-stilbene. The rotational diffusion time τ_R of the anisotropy decay (Eq. (1)) is indicated. Late spectra at the bottom reveal mainly ctD and ttD isomers and ttD triplets in acetonitrile, and a DHP-like product in n-hexane. The bleach is well fitted by difference extinction (ε_{ct} – ε_{tt}). Note the isomerization yield in acetonitrile is 4 times higher than in n-hexane.

Late spectra at the bottom of Fig. 2 correspond to photoproducts. In acetonitrile, a fit with difference extinction ($\varepsilon_{ct} - \varepsilon_{tt}$) indicates that the products are mainly ctD and ttD, with a small contribution of ttD in the triplet state. In n-hexane, a contribution from a DHP-like product is visible. Interestingly,

the isomerization yield in acetonitrile, $Y_{ttct}^{ac} = 0.40$, is 4 times greater than in n-hexane, $Y_{ttct}^{he} = 0.11$. The monoexponential decay time τ_d is calculated for bleach, SE and ESA from the corresponding band integrals presented in Fig. 3.

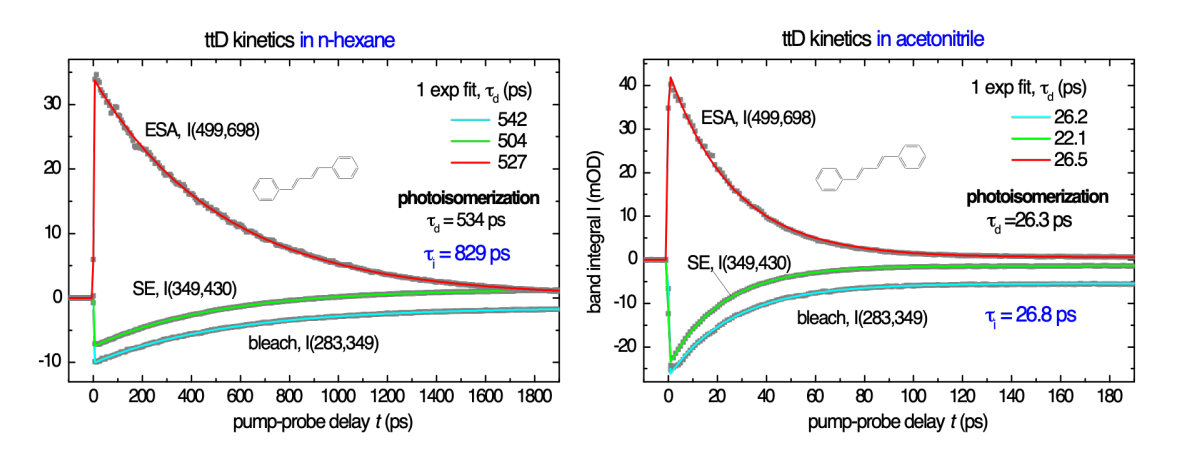


Fig. 3. ttD decay kinetics reflect $S_1 \rightarrow P$ torsion. The decays are monoexponential, as expected for a single rotamer, with decay $\tau_d = 534$ ps in n-hexane and 26.3 ps in acetonitrile, corresponding to the photoisomerization time $\tau_i = 1/(1/\tau_d - 1/\tau_{rad}) = 829$ ps and 26.8 ps, respectively. Here the radiative lifetime $\tau_{rad} = 1.5 \text{ ns}^8$ is taken the same in all our solvents. The 30-fold shortening of τ_i in acetonitrile is due to a barrier lowering of 8.4 kJ/mol (700 cm⁻¹) compared to n-hexane. Note for t-stilbene the corresponding shortening is by factor 2 only.

Note that the SE band decays faster than the bleach and ESA bands, the difference being approximately 10%. The effect is general and observed with other probe molecules like t-stilbene. We believe the reason is that the FC region for SE $(S_1 \rightarrow S_0)$ is smaller than that for ESA $(S_1 \rightarrow S_n)$. The size of the FC region along the torsion coordinate depends on the curvatures of energy surfaces S_0 , S_1 , S_n . Because S_1 is usually more parallel to S_n than to S_0 , the SE FC region is smaller; the excited wave packet then leaves it faster, resulting in the observed shortening of τ_d .

Solvent polarity and viscosity is known to dramatically affect an isomerization process, which we probed by measuring ttD in a wider range of polar and nonpolar solvents. The results are collected

in Table 1. As might be expected, the photoisomerization time τ_i increases with solvent viscosity η in nonpolar hydrocarbons, but decreases with solvent polarity f_p =[2(ϵ -1)/(2 ϵ +1)–2(n^2 -1)/(2 n^2 +1)] reflecting the polar character of the P state, similar as has been seen earlier with stilbene and stiffened stilbene derivatives. However for t-stilbene, the ratio of the isomerization times τ_i^{he}/τ_i^{ac} in n-hexane and acetonitrile is of factor 2 only, while here for ttD this ratio equals 30. Note that for many solvents, the sum of photoisomerization yields ($Y_{tt} + Y_{tt} +$

Table 1. Global Fit Results for ttD from TA with λ_{exc} =351 nm at T=20°C

solvent	$f_{ m p}$	η (cP)	τ_R (ps)	τ_d (ps)	τ_i (ps)	$Y_{tt\;tt}$	$Y_{tt\;ct}$
n-pentane (pe)	0	0.234	18.7	475	695	0.80	0.10
iso-pentane (ipe)	0	0.225	20.7	446	635	0.80	0.14
n-hexane (he)	0	0.307	23.9	529	817	0.78	0.11
n-heptane (hp)	0	0.418	29.0	574	930	0.78	0.10
iso-octane (ioc)	0	0.508	37.9	515	784	0.80	0.11
n-octane (oc)	0	0.547	35.1	597	992	0.80	0.11
n-decane (dc)	0	0.925	60.1	666	1198	0.83	0.11
cyclohexane (ch)	0	0.977	60.3	617	1048	0.84	0.10
n-hexadecane (hd)	0	3.125	163	862	2027	0.91	0.07
n-dibuthylether (db)	0.199	0.689	50.8	368	488	0.72	0.22
diethylether (de)	0.332	0.254	23.4	134	147	0.62	0.33
tetrahydrofuran (th)	0.423	0.486	41.1	109	118	0.63	0.18
acetonitrile (ac)	0.610	0.357	33.1	26.4	26.9	0.57	0.40
methanol (me)	0.618	0.587	46.2	33.4	34.2	0.56	0.36

ethanol (et) 0.579 1.186 64.3 70.6 74.1 0.60 0.36

 $f_p = [2(\epsilon-1)/(2\epsilon+1) - 2(n^2-1)/(2n^2+1)]$ – polar solvent response, ϵ – dielectric constant, n – refractive index; η – solvent viscosity coefficient, τ_R – molecular rotational diffusion time, τ_d – decay time of TA , $\tau_i = 1/(1/\tau_d - 1/\tau_{rad})$ – photoisomerization time (with $\tau_{rad} = 1.5$ ns), $Y_{tt,tt}$ and $Y_{tt,ct}$ – photoisomerization yield for ttD \to ttD and ttD \to ctD.

In order to clarify the ordering and localization of excited electronic states, 1-photon allowed $1B_u$ and 2-photon-allowed $2A_g$, we measured TA spectra of ttD in acetonitrile upon 2-photon excitation, with λ_{exc} being in the range 620-675 nm. The spectra are shown in Fig. 4, at t=2 ps on top and at 200 ps at the bottom. The signal at 2 ps strongly drops down with λ_{exc} =675 nm compared to that with λ_{exc} =620 or 652 nm, indicating the origin of $S_0 \rightarrow 2^1 A_g$ to be around 340 nm, or by 1200 cm⁻¹ higher than the $S_0 \rightarrow 1^1 B_u$ origin located at 354 nm (see Fig. 1). The obtained value differs from the previously assumed 200 cm⁻¹. Recall that in the gas phase the $2^1 A_g$ state is *below* $1^1 B_u$ by 1100 cm⁻¹. This is striking to compare with stilbene, in which 2-photon absorption has been long studied $2^{10} B_u$ also finding $1^{10} B_u$ to be the lowest-lying state in solution, with two $1^{10} A_g$ states above, one rather weak transition ~1000 cm⁻¹ above , and a stronger one ~10000 cm⁻¹ above $1^{10} B_u$.

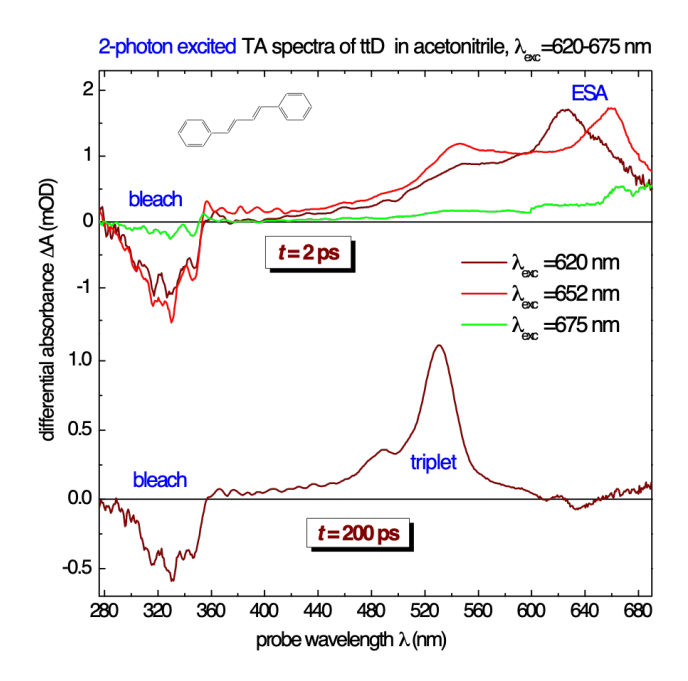


Fig. 4. TA absorption spectra of ttD in acetonitrile upon 2-photon excitation of the $S_0 \rightarrow 2^1 A_g$ transition. The signal with $\lambda_{\rm exc}$ =675 nm strongly drops down compared to $\lambda_{\rm exc}$ =620 and 652 nm. This places the origin of the transition $S_0 \rightarrow 2^1 A_g$ by ~1200 cm⁻¹ higher than $S_0 \rightarrow 1^1 B_u$ that is different from previously assumed 200 cm⁻¹.¹⁴

B. ctDPB

TA spectra and kinetics of ctD upon $\lambda_{\rm exc}$ =320 nm are shown in Figs. 5 and 6. Compared to ttD, the evolution is much faster. In n-hexane, the SE band initially rises with 1.7 ps (Fig. 5, second frame) and then decays with $\tau_{\rm d}$ =23 ps (third frame). An early blue shift of bleach and ESA, as well as the SE rise, reflect an intramolecular relaxation. The evolution occurs faster in acetonitrile, with an averaged time of 8 ps. Consider the P/SE signal: here the SE band decays with 0.7 ps reflecting half-torsion $S_1 \rightarrow P$ followed by next half-torsion and decay $P \rightarrow S_0$ with 1.7 ps (see Fig. 6). Late spectra in the bottom of Fig. 5 displays the products: the ttD and ctD isomers are well fitted by difference extinction ($\varepsilon_{\rm tt} - \varepsilon_{\rm ct}$), with a DHP-like product in n-hexane, and ttD triplet in acetonitrile.

Note that the photoisomerization yield $Y_{ct tt}$ in acetonitrile is 5 times higher than that in n-hexane, similar as with the ttD isomer.

The P-state is not distinctly observable with the ctD isomer. In n-hexane this is due to relatively slow $S_1 \rightarrow P$ transition (τ_d =23 ps), comparable to ttD in acetonitrile (τ_d =26 ps) where the P-state is also not visible. However for ctD in acetonitrile, the evolution is faster (τ_d =8 ps) and one sees indications of the P-state in the P/SE region. While in n-hexane SE and ESA rise is followed by a coordinated decay of 23 ps, in acetonitrile the decay of SE and ESA in the 354-444 nm range can be fit with ultrafast SE decay and P rise with 0.7 ps followed by the P decay of 1.7 ps (see Fig. 6). This evolution of the rising and decaying P-band, overlapping the SE region, differs from the primary ESA band centered at 622 nm and decaying with 8 ps. In particular, the exponential fitting of the band integral, as shown in Fig. 6, aids in the identification of the subtle P-state dynamics in acetonitrile.

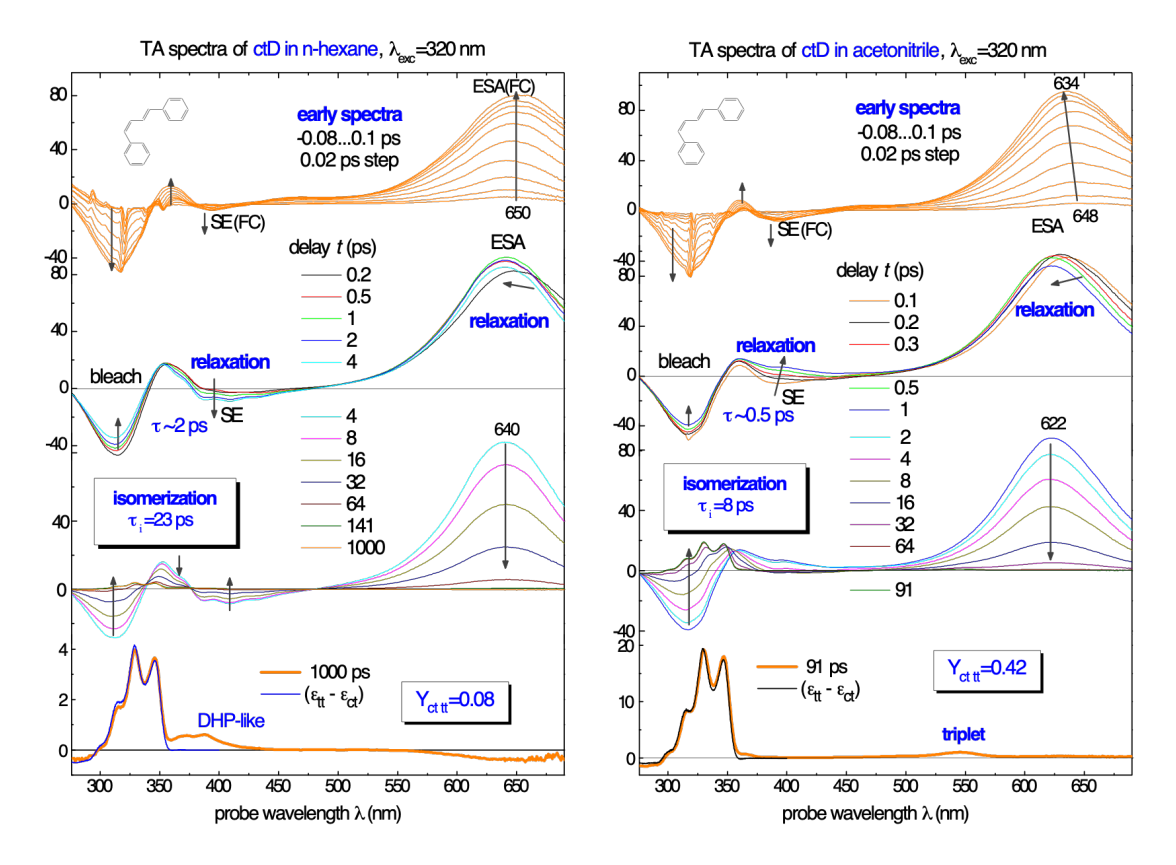


Fig. 5. TA spectra of ctD upon $S_0 \rightarrow S_1$ excitation at 320 nm. In n-hexane, the SE band rises with 1.7 ps (second frame) and decays with 23 ps (third frame). An early blue shift of ESA and bleach, and an SE rise reflect intramolecular relaxation. In acetonitrile the decay occurs with ~8 ps. In the P/SE region, the SE decay with 0.3 ps reflects $S_1 \rightarrow P$ torsion followed by $P \rightarrow S_0$ relaxation with 1.7 ps (see Fig. 6). Late spectra (bottom) reveal ttD and ctD well fitted in the bleach by difference extinction ($\varepsilon_{tt} - \varepsilon_{ct}$), ctD-triplets at 550 nm in acetonitrile, and DHP in n-hexane. Here, the negative signal in the red is due to the over-subtracted ttD contribution.

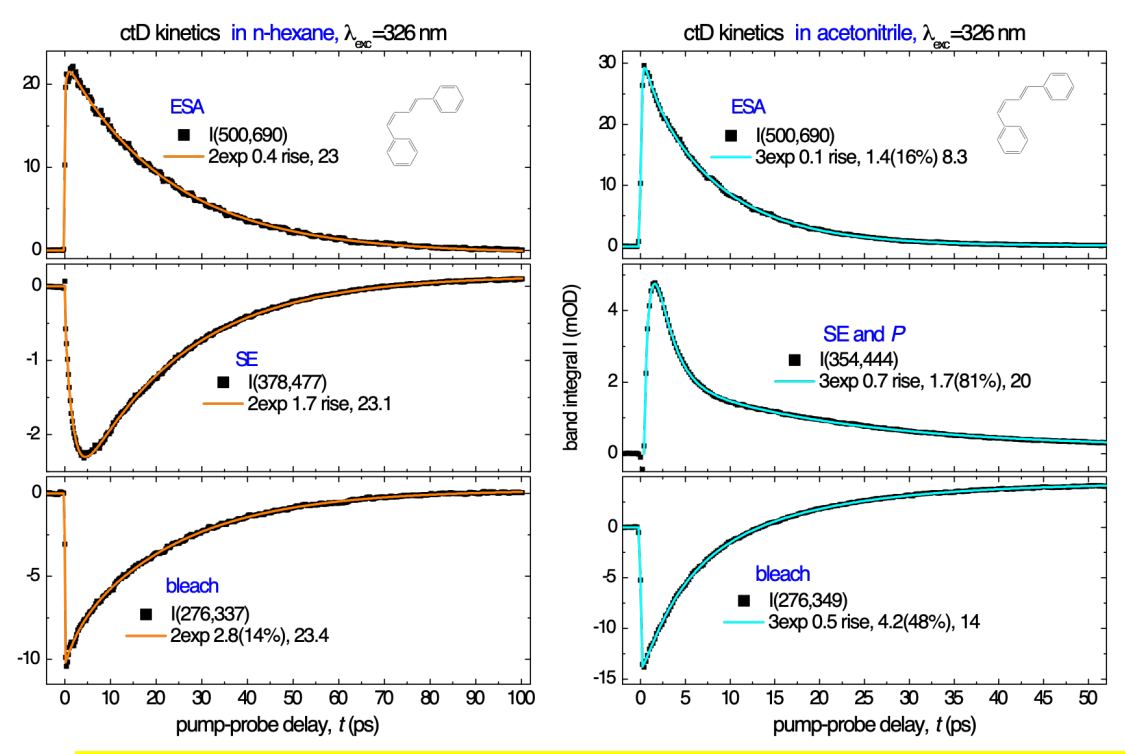


Fig. 6. The ctD kinetics in n-hexane show early SE rise with 1.7 ps and bleach decay with 2.8 ps; after 3 ps the decay is monoexponential with τ =23 ps and reflects $S_1 \rightarrow P \rightarrow S_0$ relaxation with the second step to be unresolved. In acetonitrile, SE decay and ESA rise and decay are ascribed to $S_1 \rightarrow P$ with 0.7 ps and $P \rightarrow S_0$ with 1.7 ps.

C. ccDPB

Figs. 7 and 8 show TA spectra and kinetics of ccD upon $S_0 \rightarrow S_1$ excitation at 320 nm. In this case one can directly observe the rising and decaying P-state through the ESA band at ≈ 393 nm. This P-band develops with ~ 0.2 ps (Fig. 7, second frames) in both solvents and decays with 5 ps in n-hexane and 1.6 ps in acetonitrile (third frames). In n-hexane, the red ESA band at 660 nm initially decays with 0.2 ps and then continues to decay with 5 ps simultaneously with the P-band reflecting population equilibrium between P and S_1 . The equilibrium is not reached in acetonitrile, as the ESA band decays with dual constants of 0.14 ps and 0.7 ps, but the P-state decays with 1.6 ps. Nevertheless, both solvents show remarkably clear rise and decay of their P-state, directly visible

due to a higher $P \rightarrow S_0$ barrier than the barrier $S_1 \rightarrow P$. This allows population to accumulate in the P-state, contrasting both ttD and ctD in n-hexane. Late spectra (bottom) are fitted by $(\varepsilon_{ct} - \varepsilon_{cc})$ for ctD and ccD products. Weak indications of ccD-triplets in acetonitrile and DHP n-hexane are also visible, parallel to the ttD and ctD cases. The corresponding decay kinetics and their fits are shown in Fig. 8.

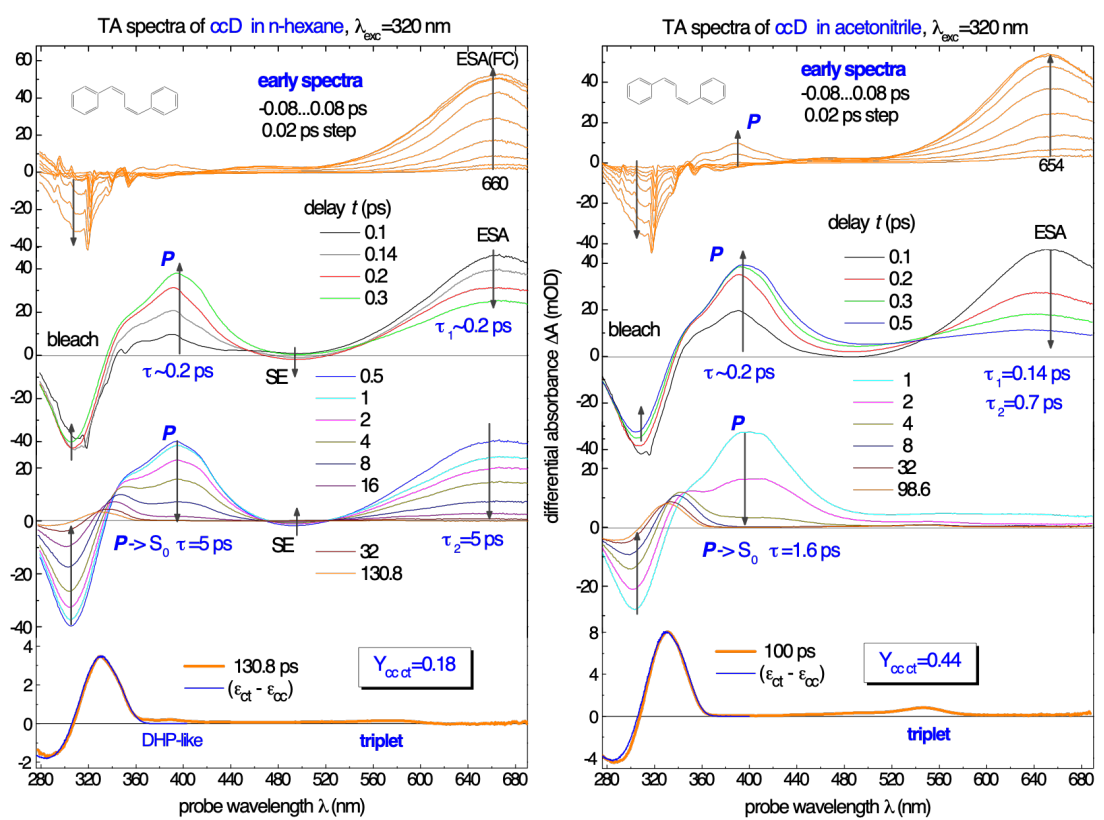


Fig. 7. TA spectra of ccD upon $S_0 \rightarrow S_1$ excitation at 320 nm. The *P*-state is observed through the rising and decaying ESA band at 393 nm. This *P*-band develops with ~0.2 ps (second frames) and decays with 5 ps in n-hexane and 1.6 ps in acetonitrile (third frames). The ESA band in n-hexane decays first with 0.2 ps, and then simultaneously with the *P*-band with 5 ps, reflecting population equilibration *PWS*₁. The equilibrium is not reached in acetonitrile where *P* decays with 1.6 ps. The late spectra (bottom) are fitted by ($\varepsilon_{ct} - \varepsilon_{cc}$). A weak negative signal in the late spectra in n-hexane is due to the over-subtracted ctD contribution.

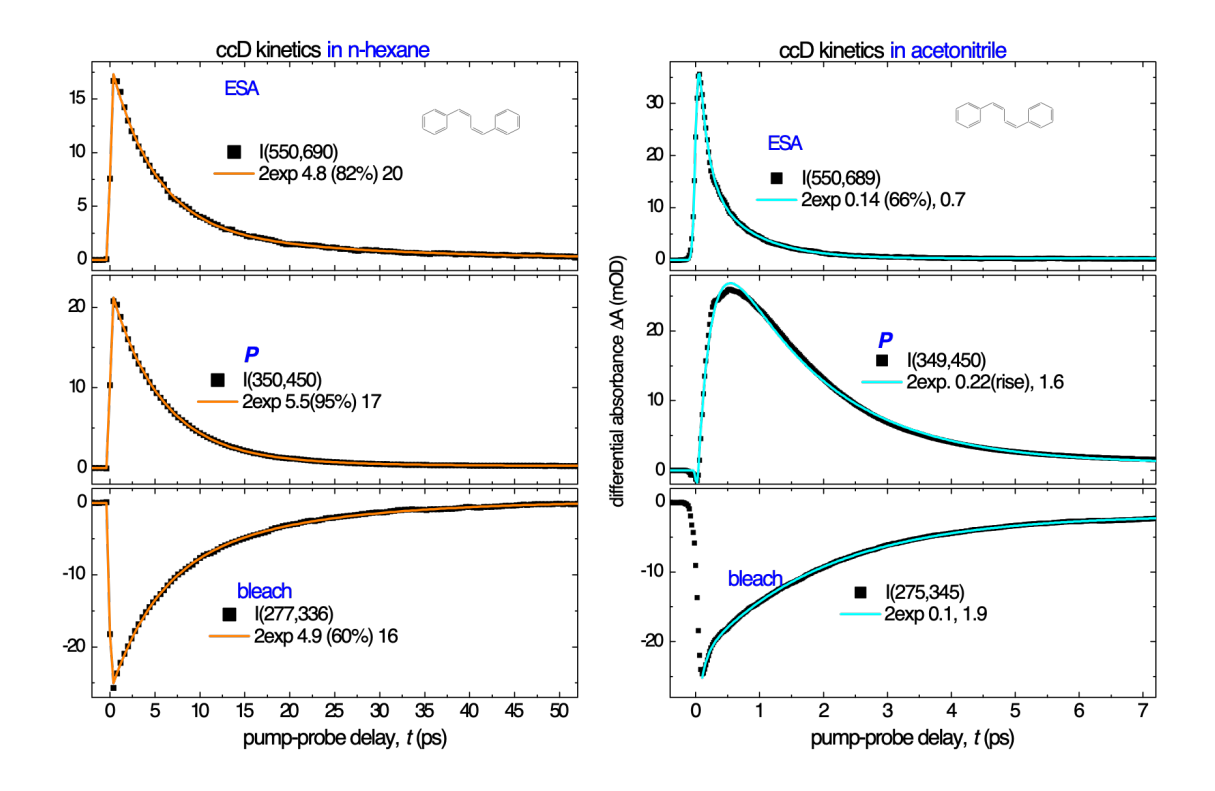


Fig. 8. ccD kinteks of ESA (top), *P*-state (middle) and bleach (bottom). The *P*-band rises with 0.15 ps and decays with 5 ps in n-hexane, and 1.6 ps in acetonitrile.

Short-time decay kinetics of ccD in n-hexane are shown in Fig. 9 at left. They are unique in comparison to ctD and ttD, and even unique to the ccD in acetonitrile solvent (Fig. 9 at right). The modulations in peak height are noteworthy as they resolve measurable oscillations between the ESA and P-state signal magnitudes. Distinctive here is the population equilibrium between P and S_1 at t > 1 ps, as the both bands decay with the same time (see Fig. 8). The observed oscillations can be attributed to the population oscillations between these two states.

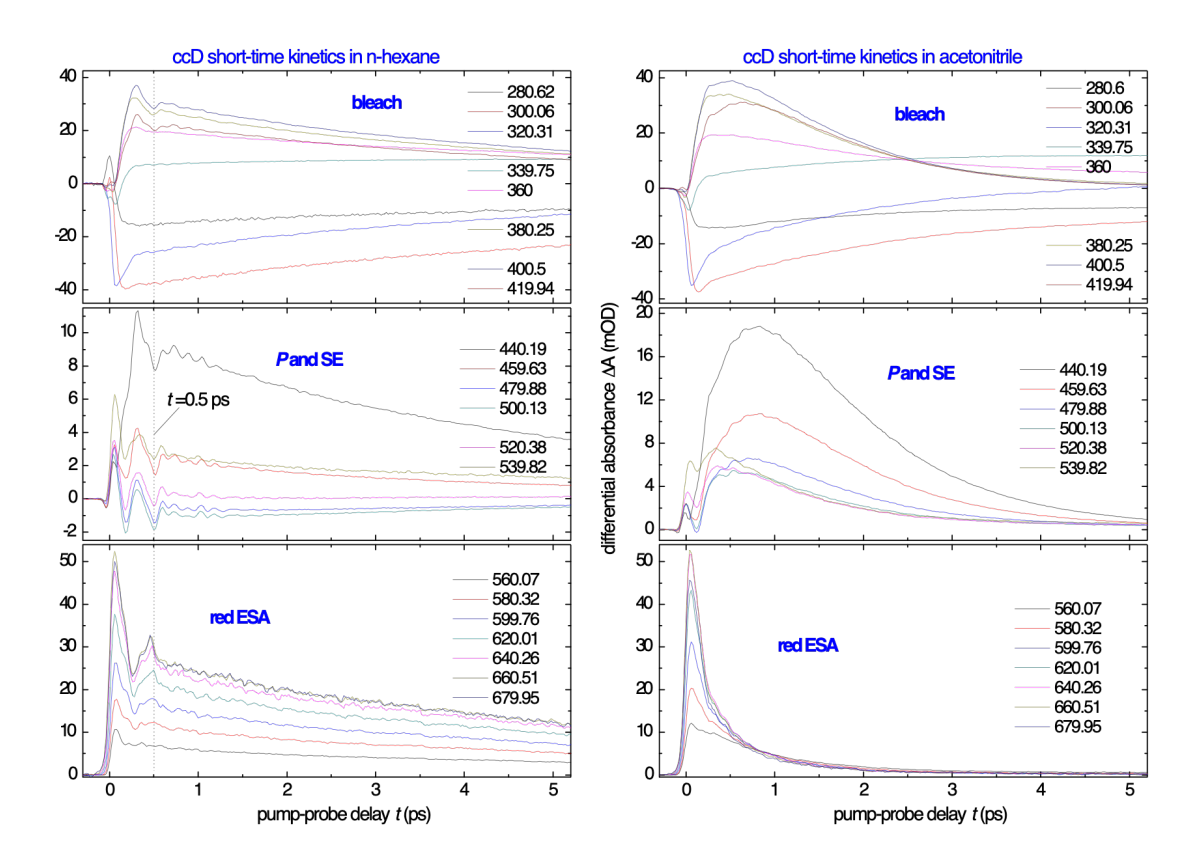


Fig. 9. Short-time decay kinetics of ccD in n-hexane (at left) reveal a strong early-time modulation that reflects the population oscillations between S_1 and P. These are not seen in acetonitrile (at right) where the oscillations are overdamped. Dashed line corresponds to 0.5 ps.

V. Computational Results and Discussion

A. Ground State: No syn-to-anti Rotamerization

It is generally accepted that DPB in S_0 prefers the *anti*-conformation of rotational isomers (rotamers) with respect to the C–C bond since the *syn*-structures suffer from unfavorable steric interactions and non-planarity associated therewith. To verify the prevalence of the *anti*-rotamers, we employ mPW2PLYP/Def2-TZVPP double hybrid DFT level which is superior to the previously reported calculations on these molecules.⁴⁷ The values obtained are summarized in Table 2.

Table 2. Relative Energy of *syn/anti-*Rotamers (mPW2PLYP/Def2-TZVPP)

Isomer/rotamer	Energy, kJ/mol				
trans-anti-trans	0.0				
trans-syn-trans	16.9				
trans-anti-cis	11.8				
trans-syn-cis	34.3				
cis-anti-cis-C2	22.4				
$cis-anti-cis-C_i$	28.7				
cis-syn-cis	45.0				

Most of the structures have only one stationary point, with trans-phenyl(s) in-plane with the adjacent double bond and cis-phenyl(s) some 35° out-of-plane due to H-H repulsion. The only exception is the cis-*anti*-cis conformation where matched or opposing rotations of the phenyl rings give rise to the two distinct local minima.

As follows from the estimates of Table 2, the equilibrium room-temperature fraction of the *syn*-rotamers in the ground state is about 0.1% or even lower. The rotamer equilibrium is ensured by very low rotation barriers typical of single bonds in conjugated systems: the activation energy for the trans-*syn*-trans to trans-*anti*-trans rotation was calculated to be only 22 kJ/mol. . Hence, the initially excited ensemble contains only the *anti*-rotamers, and our further computational results will refer to them without an explicit indication. Like in stilbene each trans-to-cis transition in the *anti*-rotamer is energetically disfavored by 10-12 kJ/mol.

B. Excited States in ttD

As already indicated above, 2-photon-excitable 2^1A_g and 1-photon-excitable 1^1B_u states in DPB change their order on going from gas to liquid. In the gas phase, the origin of 2^1A_g is about 1150 cm⁻¹ lower, ¹⁰⁻¹² but the order is inverted in liquid solution where the 1^1B_u emerges as S_1 . This is commonly explained by the higher polarizability of 1^1B_u . ¹⁴ To investigate the issue, we optimize the two excited states at the XMCQDPT2 level and calculate their polarizability via numerical differentiation of energy over the electric field.

At the S_0 geometry, the 1^1B_u state is found below 2^1A_g by 0.28 eV, in a seeming disagreement with the gas-phase experimental results. 1^{10-12} The XMCQDPT2 vertical excitation energy for the two states are, respectively, 3.77 and 4.05 eV. However, optimization of the stationary points on the S_1 and S_2 surfaces provides the results in line with the experiment. Thus, the S_1 stationary point corresponds to the 2^1A_g electronic state, the 0-0 transition being 3.56 eV, while the S_2 stationary point corresponds to 1^1B_u which is found 0.16 eV higher. These are in good agreement with the jet experiments. 1^{10-12} It appears to be locally stable with respect to possible symmetry-breaking interaction with 2^1A_g , despite even smaller vertical gap of only 0.05 eV. The 2^1A_g state shows a greater geometrical deviation from S_0 than 1^1B_u , hence its stronger relaxation in terms of energy is expected. The both structures retain planarity and C_{2h} symmetry (see Supporting Information). This is in contradiction with the recent CASSCF(4,4) results supplemented with single-point ICMRCI recalculations 1^{10} that locate no planar minima in S_1 (of unspecified electronic structure) and report only a highly twisted one. However the experimental data clearly favors our findings.

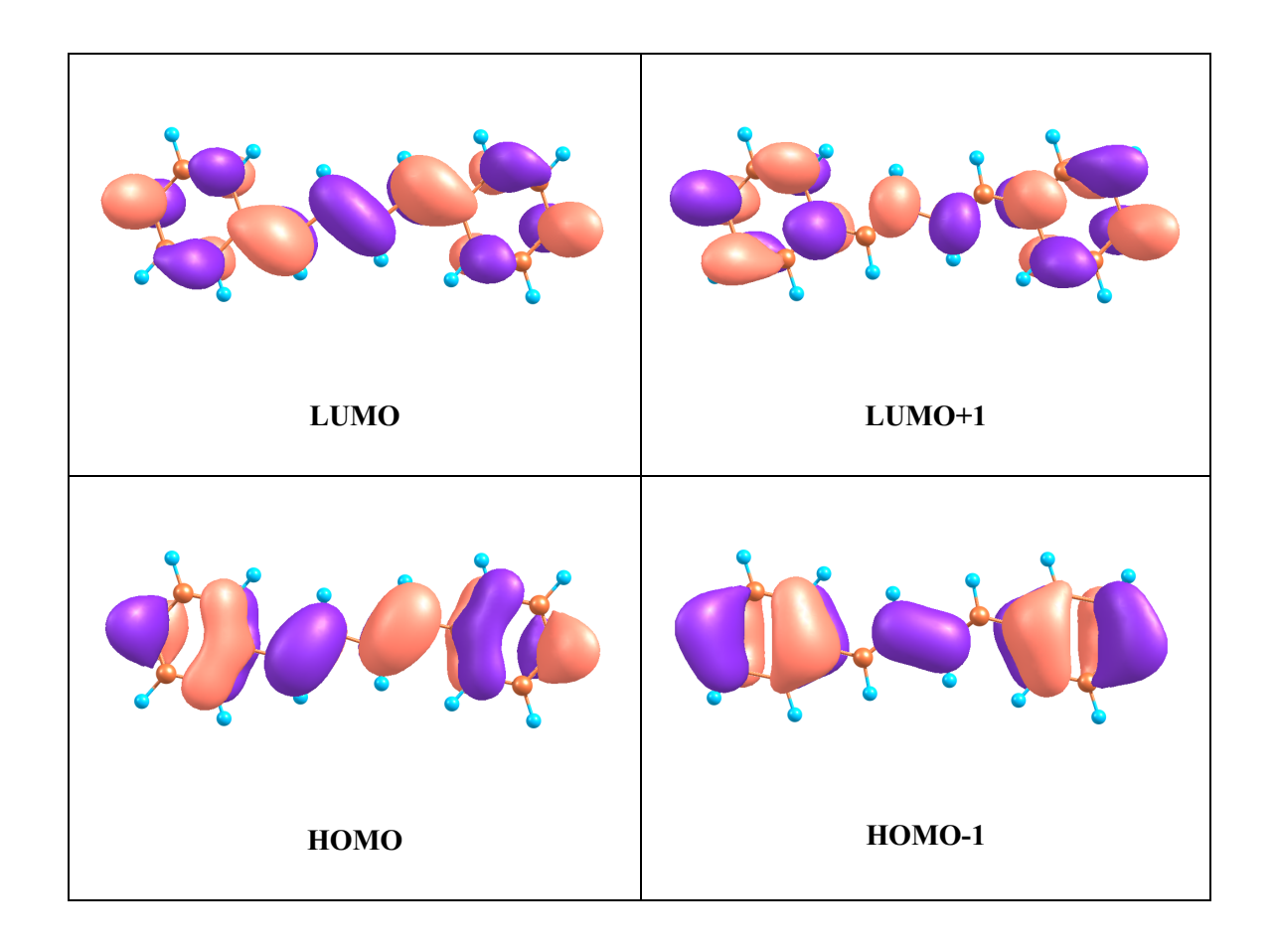


Fig. 10. The four frontier orbitals involved in the principal electronic configurations in the lowest excited states of ttD.

In agreement with the current consensus and expectations, the 1^1B_u state is dominated by the single HOMO \rightarrow LUMO excitation (ca. 80%). The major contributions to 2^1A_g include 30% of the double (HOMO) $^2\rightarrow$ (LUMO) 2 excitation and two single excitations, HOMO-1 \rightarrow LUMO and HOMO \rightarrow LUMO+1, about 15% each. The above four frontier orbitals are shown in Fig. 10. Even though there are two equivalent double bonds between the phenyl rings, the HOMO and LUMO are pronouncedly separated from the rest of the frontier orbitals including the HOMO-1 and LUMO+1. The HOMO has a bonding character with respect to the double bonds while the LUMO is anti-bonding with respect to these bonds and, accordingly, bonding with respect to the single

Ph–C and C–C bonds. As a result, the lengths of the single and double bonds in both 1^1B_u and 2^1A_g states tend to equalize.

Dipole coupling of closely located 1^1B_u and 2^1A_g inevitably enhances polarizability in the lower of them, in 2^1A_g in the gas phase (jets) or in 1^1B_u in liquid solution, at the expense of the higher one. For instance, the gas phase polarizability of 1^1B_u at its stationary point is even lower than that of 2^1A_g . Therefore, it is more instructive to compare the polarizability of the two states after subtracting the term responsible for their interaction, i.e. the squared transition dipole related to the energy gap. This "corrected" isotropic polarizability is adequately stable with respect to the molecular geometry variations and appears to be about twice as high in the optimized 1^1B_u state, $76 \text{ Å}^3 \text{ vs. } 36 \text{ Å}^3 \text{ in } 2^1A_g$. Interestingly, the ground state value of 61 Å^3 happens to be higher than even the average over the two excited states. Thus, reordering of the excited states in solution can indeed be explained by the polarizability effects. The higher polarizability of the 1^1B_u state in solution results from the dipole coupling to one of the 1^1A_g states located higher by 1.8 eV. This 1^1A_g includes the same principal configurations as 2^1A_g , but with inverted signs at the single excitations. The transition dipole moment between the coupled states reaches 19-20 D depending on the molecular geometry.

C. Excitation/Emission Energies and Isomerization Barriers in S_1

From our previous studies 45,46,48 the relevant S_1 state of stilbene and many of its symmetric derivatives is dominated by the single HOMO \rightarrow LUMO excitation, and it can be properly described using a more cost-efficient TDDFT treatment. The doubly excited states do not interfere in stilbenes, and S_1 retains its single-excited character along the twisting coordinate until it reaches the trans-to-cis or cis-to-trans isomerization barrier. Between the two barriers, in the central perpendicular domain of S_1 (known as the phantom state P) conventional linear response TDDFT breaks down and only sin-flip TDDFT remains applicable. 50

For DPB, the gas phase S_1 state, with its higher contribution of the double $(HOMO)^2 \rightarrow (LUMO)^2$ excitation, is not treatable by the conventional TDDFT. As a rather successful remedy, a dressed TDDFT approach has been reported. However in liquid solution, single-excited 1^1B_u becomes S_1 and one can return to the conventional TDDFT approach that describes the 1^1B_u correctly.

The isomerization barrier of ttD in hexane measured herein does not exceed 1900 cm⁻¹ (see Table 4 below), higher than ≈ 1050 cm⁻¹ in the 2^1A_g state^{11,12} for the isolated molecule. But the origin of 2^1A_g in n-hexane is 1200 cm⁻¹ above 1^1B_u (see Sec. 4.1), which attributes the measured barrier to the 1^1B_u . We therefore denote below the relevant 1^1B_u excited state as S_1 .

Vertical $S_0 \rightarrow S_1$ excitation energy, $S_1 \rightarrow S_0$ emission energy, 0-0 transition energies, and relative energy at the stationary points calculated at the TD-PBE0/Def2-TZVPP level (with mPW2PLYP S_0 geometries) are summarized in Table 2. For ccD, the slightly more stable C_2 conformation is selected as a starting point. Generally, ttD and the trans-side of ctD remain planar, in agreement with the XMCQDPT2 data, while in the cis-halves the coordination of the double bonds becomes less planar (like in stilbene³⁸) in favor of the adjacent single bonds whose order increases in S_1 . The values of Table 3 are 0.2 eV lower than the peak energies in alkanes. As one can see, the relative energies in S_1 resemble those of S_0 (compare with Table 1), likely due to the same steric reasons. Note, however, that the energy dependence on the number of cis-fragments is now not linear.

Table 3. Vertical Excitation (E_{abs}), Vertical Emission (E_{em}), 0-0 Transition (E_{0-0}) Energy, and Relative Energy (E_{rel}) of S_1 from TD-PBE0/Def2-TZVPP

Conformation	E _{abs} , eV	E _{em} , eV	E ₀₋₀ , eV	$E_{rel}(S_1)$, kJ/mol
ttD	3.60	3.13	3.35	0.0
ctD	3.72	3.01	3.32	10.9
ccD	3.88	3.07	3.42	31.6

The relaxed torsional scans reveal that even in the symmetric trans-trans and cis-cis conformation the two possible torsions are decoupled, i.e. when one double bond is being twisted the second one does not follow it and remains planar. The HOMO and LUMO, however, keep almost equally delocalized over the both double bonds, the one being twisted and the one remaining planar. The respective optimized photoisomerization barriers E_a are shown in Table 4, together with the experimental barriers E_{1a} estimated as

$$E_{1g} = RT \cdot ln(\tau_i/\tau_0) \tag{5}$$

Here $\tau_0 = 0.1$ ps for barrierless isomerization is taken from our previous studies of stilbene⁴¹ and its derivatives, 43-46 the photoisomerization time τ_i is from Table 1, and RT=2.436 kJ/mol. In ccD, simultaneous decay of the ESA and P band after ultrafast partial population of P suggests that S_1 and P are in equilibrium with interconversion rates significantly faster than the decay rate. As seen, the agreement between the experiment and calculations is reasonable.

Table 4. Calculated (E_a) and Experimental (E_{1a}) Photosomerization Barriers in S_1 and Torsional Angles at the Equilibrium Geometry and in the Transition State

photoisomerization	Ea (TD-PBE0)	E_{1a} (exp)	Equilibrium	Torsional angle in
path	kJ/mol	kJ/mol	torsional angle, deg	transition state, deg
$ttD \rightarrow ctD$	26.4	22.0	180.0	121.2
$ctD \rightarrow ccD$	26.3	-	177.1	121.8
$ctD \rightarrow ttD$	13.5	13.3	17.6	62.2
$ccD \rightarrow ctD$	4.4	<5.6	20.5	59.8

The extent of non-planarity at the transition state is almost the same in all cases. Trans-to-cis twisting is calculated to have virtually the same barrier in ttD and ctD, but the cis-to-trans barrier in ctD is much lower, and we, accordingly, cannot observe production of ccD from ctD in the transient spectra. In general, the barrier heights of Table 4 are governed by the energy at the respective minima where the amount of steric interactions differs between the cis and trans configurations (see the rightmost column of Table 3) rather by the energy at the transition state where the steric differences are much reduced. Compared to our experimental findings below, the barrier heights seem at least to correctly reproduce the relative trends.

At the TDDFT level, anti-syn rotation around the central C–C bond is found irrelevant in S_1 , the respective barrier in ttD reaching 117 kJ/mol. However, this possibility obviously requires further attention in the light of observation of the DHP-like products. When the conformation at the central single bond is *anti*, rather than *syn*, as it is in S_0 , there is merely no opportunity for cyclization. Therefore, if the assignment of the presumed DHP bands is correct, *anti*-to-*syn* rotations can take place in excited DPB, and our preliminary XMCQDPT2 data also support that possibility. Furthermore, an extra degree of freedom may be behind the biexponential behavior in ctD and ccD. However, such *anti*-to-*syn* rotations may occur only after reaching the P state. Also the 2^1A_g state might be involved.

D. Solvent Effects and the P State

The experimental results in different solvents are summarized in Table 5, including peak wavelengths and decays of bleach, SE, ESA and P-band of the DPB and stilbene isomers. Several trends emerge, some familiar to previous experiments, and others specific to DPB. For example, the isomerization time (τ_{ESA}) is shorter in acetonitrile than in hexane, which was observed before in stilbene, as well as in substituted and stiffened stilbenes. Perhaps more striking is the strong dependence of τ_i on the solvent polarity, as demonstrated by Table 1. By measuring the

isomerization of ttD in a range of solvents, dependence on both viscosity and polarity can be discerned. That is, the less viscous and more polar the solvent is, the faster the isomerization will be. The viscosity dependence is perhaps intuitive: a twisting motion will face greater resistance with greater viscosity. On the other hand, the polarity dependence is typically interpreted as stabilization of a zwitterionic P-state, indicated also by a blue-shift in the P-state absorption band in acetonitrile as compared to hexane. Interestingly, the blue-shift of the P absorption in acetonitrile is much smaller than the \sim 500 cm⁻¹ blue-shift of ESA (see Fig. 11). The same behavior is also seen in unsubstituted stilbene, though in some substituted stilbenes this may be inverted. A possible explanation is that the P state is coupled to higher excited states that are likewise polar.

Also notable is the rise and decay of the P-state. In general, photoisomerization does not necessarily have a directly observable P-state. It is more likely to be observed from a cis-to-trans isomerization, as was originally observed in stilbene. If the P-state is observable, then one can infer that an $P \rightarrow S_0$ barrier is larger than or comparable to the $S_1 \rightarrow P$ barrier. A long-lived P-state coincides with a heightened barrier to the P/S_0 conical intersection, most striking in a recent comparison of stiffened stilbene derivatives. For ctD in acetonitrile the P-state is visible, while it is not apparent in n-hexane. This is likely because the $S_1 \rightarrow P$ isomerization is much slower than the $P \rightarrow S_0$ rate, as is in the case for ttD. In contrast, the $S_1 \rightarrow P$ torsion of ctD is much faster in acetonitrile, and a notable $P \rightarrow S_0$ barrier exists, allowing a P-state population to accumulate, as is in ccD as well. In ccD, similarly to cis-stilbene, the $P \rightarrow S_0$ torsion is even faster than $S_1 \rightarrow P$ isomerization, so it provides the best opportunity to observe the characteristic behavior of P.

For ccD in n-hexane, the lower barrier produces a unique effect: it results in simultaneous decay of the S_1 and P-state. This implies population equilibrium between S_1 and P, and finely resolved ultrafast dynamics of the two populations. Fig. 9 contrasts bands of ESA, P-state and bleach for ccD in n-hexane and acetonitrile. Noteworthy are the 2 cycles of oscillations visible in n-hexane but absent in acetonitrile, with a half-period phase difference between the S_1 (ESA) oscillations and

the P-state oscillations. This should reflect oscillations of the population between the two nearly isoenergetic states before settling into an equilibrium. In acetonitrile, stabilization of the P state considerably shifts or even destroys the equilibrium. As is shown by the calculations (Table 4) equilibration is facilitated by a low torsional barrier.

A quite similar behavior has been observed for cis-stilbene in n-hexane. There, an ultrafast subpicosecond decay of S_1 and concomitant rise of P is followed by their simultaneous 1 ps decay, the population of S_1 and P being in equilibrium but not showing the oscillations observed in ciscis-DPB.

Table 5. Bleach, SE, and ESA Peaks, Decay (d) and Rise (r) Time Contants, and Yields

	Bleach λ _{bl} τ _{bl}		SE λ _{SE} τ _{SE}		ESA λεsa τεsa		$P = \lambda_P = au_P$		isomer ization
	(nm)	(ps)	(nm)	(ps)	(nm)	(ps)	(nm)	(ps)	yield Y
ttD he	328	542	504	504	649	527			tt→ct 0.1
ttD ac	328	26	22	22	624	27			tt→ct 0.56
ctD he	312	23	410	1.7 r 23 d	641	23			ct→tt 0.08
ctD ac	318	8	397	0.3	620	8		1.2 r 8 d	ct→tt 0.42
ccD he	303	8	480	0.1	664	5	393	0.2 r 5 d	cc→ct 0.18
ccD ac	305	4		0.1	638	0.3	395	0.2 r 1.6 d	cc→ct 0.44
tSt he	300	84	350	84	583	84			t→c 0.5
tSt ac	300	40	350	40	577	40			t→c 0.5
cSt he					632	1.2	338	0.3	c→t 0.5
eSt ac					626	0.8	340	0.2 r 0.8 d	c→t 0.37

"he" stays for n-hexane, and "ac" - for acetonitrile

It is interesting to compare the P-decay in ccD to to that in cis-stilbene (cSt), as this yields information about the conical intersection. For example, in stilbene the yield is nearly 50% for each solvent and isomer. However, in ccD the isomerization to ctD in acetonitrile is 3 times more likely than in n-hexane, where the ccD isomer mainly returns to S_0 . This is reflective of a shift in the conical intersection, altering the relative barriers of the P-state to either isomer. Indeed for all isomers of DPB, isomerization is more likely in acetonitrile than in n-hexane by at least a factor of two.

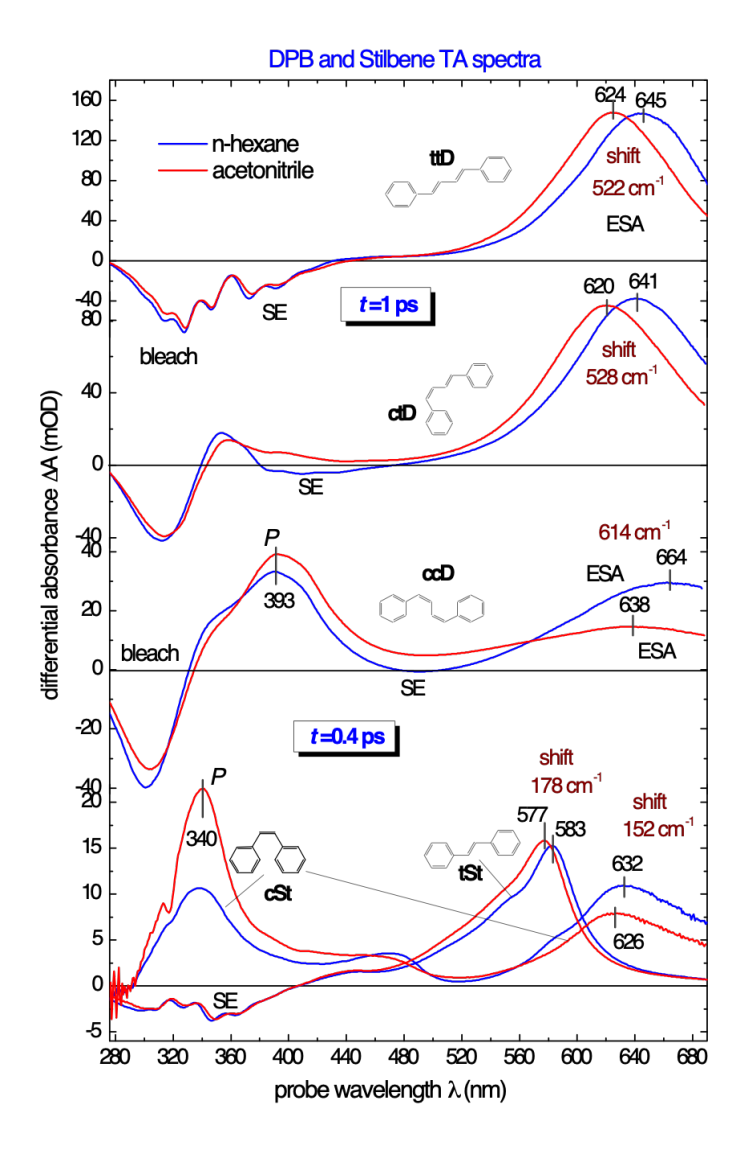


Fig. 11. TA spectra of DPB (top three frames) and of stilbene (St) (in the bottom). The DPB spectra are recorded upon λ_{exc} =320 nm, with excess energy for ttD, resulting in reduced SE compared to bleach. The spectra of ttD, ctD, tSt are taken at t=1 ps, and those of ccD, cSt at t=0.4 ps. The tSt spectrum (λ_{exc} =326 nm) is scaled down by factor 10 compared to the spectrum of cSt (λ_{exc} =315 nm).

A second feature of the perpendicular state is that its lifetime is by factor 3 longer in n-hexane over acetonitrile (Table 5). A reduction in the relative P-state energy is expected in polar solvents, since experiment and theory on similar molecules suggest a zwitterionic P-state. Yet this can decrease the barrier from the P-state to the conical intersection, as exemplified in Fig. 12. As can be seen from this diagram, stabilization of the P-state decreases both the $S_1 \rightarrow P$ and $P \rightarrow S_0$ barrier heights,

thus dramatically altering the dynamics. This demonstrates that acetonitrile can consistently reduce the photoisomerization barrier for both DPB and stilbene, yet has an effect on the perpendicular state lifetime that varies from system to system.

In a conventional model with two parabolic wells as shown in Fig. 12, reduction of the S_1/P barrier in polar solvents is always smaller than the solvation energy of the P state. Conversely, the barrier heights provide an estimate from below for the P stabilization in acetonitrile relative to n-hexane according to

$$\Delta E > RT \ln(\tau_i^{he}/\tau_i^{ac}) = 7.3 \text{ kJ/mol} = 620 \text{ cm}^{-1}$$
 (6)

Relating the estimate (6) to solvation energy $E_{solv} = f\mu_p^2/2a^3$ of a point dipole μ_P in a spherical cavity of radius a, $f = 2(\varepsilon - 1)/(2\varepsilon + 1)$, and the solute polarizability being neglected, one gets

$$(f_{ac} - f_{be})\mu_P^2/2a^3 > 620 \text{ cm}^{-1}, \qquad \mu_P > 9.6 \text{ D}$$
 (7)

Here a=6 Å is taken for DPB, and we make use of the relation: $1 \text{ D}^2/\text{Å}^3 = 5032 \text{ cm}^{-1}$. In view of the previous computational results for the P state of stilbenes, 46,48 this estimate seems too conservative, and $\mu_P \sim 20 \text{ D}$ for DPB is more likely.

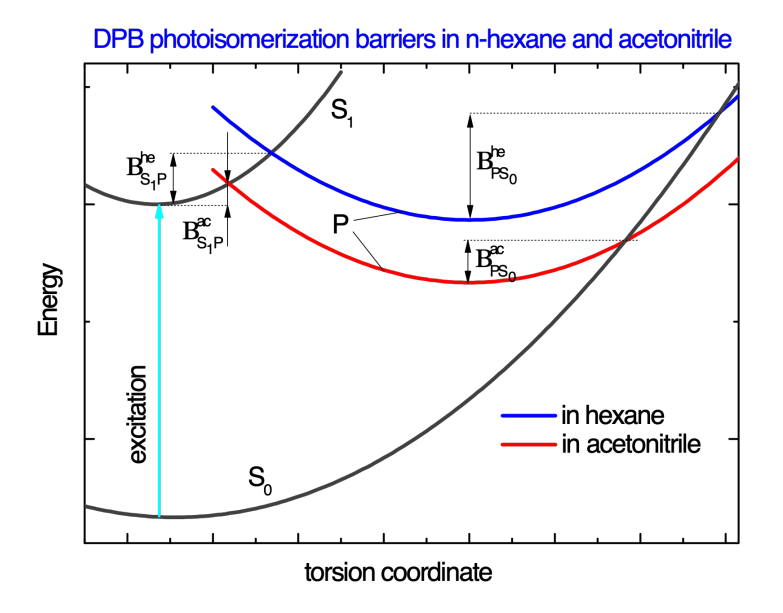


Fig. 12. Photoisomerization barriers in acetonitrile and n-hexane. Diabatic S_1 and P surfaces of ttD, ctD or ccD correspond to optically excited $(S_0 \rightarrow S_1)$ and perpendicular state P. The "B" denotes a barrier, with solvent in the superscript, and initial and final state in the subscript.

VI. Conclusion

In conclusion we have studied the photoisomerization dynamics of three isomers of DPB. 2-photon excited TA spectra of ttD demonstrate that in solution the $2A_g$ state is located 1200 cm⁻¹ higher than 1-photon allowed $1B_u$ (S_1), the estimate being obtained for the first time. The calculated barriers agree with the experiment and with the observation that ctD isomerize mainly to ttD and not to ccD. The P-state with its characteristic band at 392 nm is discernible in ccD due to ultrafast $S_1 \rightarrow P$ torsion, with a measurable decay both in n-hexane and acetonitrile. For ccD in n-hexane, fast decaying oscillations are observed between the S_1 and P population, followed by a simultaneous decay of these states. Solvent effects are studied for ttD, demonstrating faster isomerization in polar solvents and in less viscous solvents. This is also seen in the comparison of each isomer's dynamics in n-hexane contrasted with acetonitrile. The photoisomerization rate of ttD in acetonitrile is 30

times faster than in n-hexane, while for t-stilbene the corresponding rates differ by factor 2 only. The isomerization yields of DPB in acetonitrile are $2\div5$ times higher than in n-hexane while in stilbene the yields are near even. The present results are consistent with a highly polar *P*-state (μ_P ~20 D), anticipated by theory and experiment on similar systems.

This work expands upon previous experiments focused only on ttD, and allows comparison of each isomer, photoisomerization between them, and comparison with stilbene and substituted stilbene compounds.

Acknowledgement

This paper is devoted to the memory of Alex Granovsky.

O. A. K. thanks the National Science Foundation under grant CHE 1900226.

I. N. I. and S. M. S. thank the Russian Foundation for Basic Research for financial support; grant 19-33-90252.

The calculations were carried out using the facilities of HPC computing resources at Lomonosov Moscow State University.

References

- 1. M. T. Allen, D. G. Whitten, Chem. Rev. 89, 1691 (1989).
- 2. J. H. Pinckard, B. Wille, L. A. Zechmeister, J. Am. Chem. Soc. 70, 1938 (1948).
- 3. W. A. Yee, S. J. Hug, D. S. Kliger, J. Am. Chem. Soc. 110, 2164 (1988).
- 4. S. P. Velsko, G. R. Fleming, J. Chem. Phys 76, 3553 (1982).
- 5. S. H. Courtney, G. R. Fleming, Chem. Phys. Lett. 103, 443 (1984).
- M. Lee, A. J. Bain, P. J. McCarty, C. H. Han, J. N. Haseltine, A. B. Smith III, and R. M. Hochstrasser, J. Chem. Phys. 85, 4341 (1986).
- 7. R. M. Anderton and J. F. Kauffman, J. Phys. Chem. 98, 12125 (1998).
- 8. K. Dahl, R. Biswas, and M. Maroncelli, J. Phys. Chem. 107, 7838 (2003).
- 9. J. Schroeder, T. Steinel, J. Troe, J. Phys. Chem. A 106, 5510 (2002).
- 10. L. A. Heimbrook, B. E. Kohler, and T. A. Spiglanin, Proc. Natl Acad. Sci. USA 80, 4580 (1983).
- 11. J. F. Shepanski, B. W. Keelan, and A. H. Zewail, Chem. Phys. Lett. 103, 9 (1983).
- 12. A. Amirav, M. Sonnenschein, and J. Jortner, J. Chem. Phys. 102, 305 (1986).
- 13. T. Itoh. Chem. Phys. Lett. 342, 550 (2001).
- 14. T. Itoh, Y. Numata, I. Suzuka, Chem. Phys. Lett. 445, 179-182 (2007).
- 15. W. Mizukami, Y. Kurashige, M. Ehara, T. Yanai, and T. Itoh, J. Chem. Phys. 131, 174313 (2009).
- J. Saltiel, T. S. R. Krishna, K. Laohhasurayotin, Y. Ren, K. Phipps P. H. Davis and W. A. Yee, J. Phys. Chem. A, 115, 2120 (2011).
- 17. J. S. Baskin, L. Bañares, S. Pedersen, A. H. Zewail, J. Phys. Chem. A, 100, 11920 (1996).
- 18. L. R. Khundkar, R. A. Marcus, and A. H. Zewail, J. Phys. Chem. 87, 2473 (1983).
- 19. H. A. Kramers, *Physica* 7, 284 (1940).
- 20. D. G. Truhlar, B. C. Garrett, and S. J. Klippenstein, J. Phys. Chem. 100, 12771 (1996).

- 21. P. Hänggi, P. Talkner, M. Borkovec, Rev. Mod. Phys. 62, 251 (1990).
- 22. G. R. Fleming, S. H. Courtney, and M. W. Balk, J. Stat. Phys. 42, 83 (1986).
- 23. D. H. Waldeck, Chem. Rev. 91, 415 (1991).
- 24. D. M. Leitner, B. Levine, J. Quenneville, T. J. Martinez, P. G.Wolynes, J. Phys. Chem. A 107 10706 (2003).
- 25. J. Quenneville, T. J. Martinez, J. Phys. Chem. A 107, 829 (2003).
- 26. L. Houk, I. L. Zheldakov, T. A. Tommey, C. G. Elles, J. Phys. Chem. B 28, 9335 (2015).
- 27. A. Meyer, J. Schroeder, and J. Troe, J. Phys. Chem. A, 103, 10528 (1999).
- 28. K. Fuke, S. Sakamoto, M. Ueda, M. Itoh, Chem. Phys. Lett. 74, 546 (1980)
- 29. G. Hohlneicher, B. Dick, J. Photochem. 27, 215 (1984)
- 30. G. Hohlneicher, R. Wrzal, D. Lenoir, R. Frank, J. Phys. Chem. A 103, 8969 (1999)
- 31. M. de Wergifosse, A. L. Houk, A. I. Krylov, C. G. Elles, J. Chem. Phys. 146, 144305 (2017).
- 32. J. Bao, P. M. Weber, J. Phys. Chem. Lett. 1, 224 (2010).
- 33. A. A. Granovsky, Firefly v. 8.2, http://classic.chem.msu.su/gran/firefly/index.html
- 34. M. W. Schmidt, K. K. Baldridge, J. A. Boatz, S. T. Elbert, M. S. Gordon, J. H. Jensen, S. Koseki, N. Matsunaga, K. A. Nguyen, S. Su, T. L. Windus, M. Dupuis, J. A. Montgomery, J. Comput. Chem. 14, 1347 (1993).
- 35. Gaussian 09, Revision D.03, M. J. Frisch, G. W. Trucks, H. B. Schlegel, G. E. Scuseria, M. A. Robb, J. R. Cheeseman, G. Scalmani, V. Barone, B. Mennucci, G. A. Petersson, H. Nakatsuji, M. Caricato, X. Li, H. P. Hratchian, A. F. Izmaylov, J. Bloino, G. Zheng, J. L. Sonnenberg, M. Hada, M. Ehara, K. Toyota, R. Fukuda, J. Hasegawa, M. Ishida, T. Nakajima, Y. Honda, O. Kitao, H. Nakai, T. Vreven, J. A. Montgomery, Jr., J. E. Peralta, F. Ogliaro, M. Bearpark, J. J. Heyd, E. Brothers, K. N. Kudin, V. N. Staroverov, R. Kobayashi, J. Normand, K. Raghavachari, A. Rendell, J. C. Burant, S. S. Iyengar, J. Tomasi, M. Cossi, N. Rega, J. M. Millam, M. Klene, J. E. Knox, J. B. Cross, V. Bakken, C. Adamo, J. Jaramillo, R. Gomperts, R. E. Stratmann, O. Yazyev, A. J. Austin, R. Cammi, C. Pomelli, J. W. Ochterski, R. L. Martin, K. Morokuma, V. G. Zakrzewski, G. A. Voth, P. Salvador, J. J. Dannenberg, S. Dapprich, A. D. Daniels, Ö. Farkas, J. B. Foresman, J. V. Ortiz, J. Cioslowski, and D. J. Fox, Gaussian, Inc., Wallingford CT, 2009.
- 36. Granovsky, A. A. J. Chem. Phys. 134, 214113 (2011).

- 37. S. A. Kovalenko, A. L. Dobryakov, I. Ioffe, N. P. Ernsting, Chem. Phys. Lett. 493, 225 (2010).
- 38. S. A. Kovalenko, R. Schanz, H. Hennig, N. P. Ernsting, J. Chem. Phys. 115, 3256 (2001).
- 39. V. Karunakaran, K. Kleinermanns, R. Improta, S. A. Kovalenko, J. Am. Chem. Soc. 131, 5839 (2009).
- J. Moreno, A. L. Dobryakov, I. N. Ioffe, A. A. Granovsky, S. Hecht, S. A. Kovalenko, J. Chem. Phys.
 143, 024311 (2015).
- 41. S. A. Kovalenko, A. L. Dobryakov, I. Ioffe, N. P. Ernsting, Chem. Phys. Lett. 493, 225 (2010).
- 42. I. N. Ioffe, M. Quick, M. T. Quick, A. L. Dobryakov, C. Richter, A. A. Granovsky, F. Berndt, R. Mahrwald, N. P. Ernsting, S. A. Kovalenko, J. Am. Chem. Soc. 139, 15265 (2017).
- 43. A. L. Dobryakov, M. Quick, C. Richter, C. Knie, I. N. Ioffe, A. A. Granovsky, R. Mahrwald, N. P. Ernsting, S. A. Kovalenko, J. Chem. Phys. 146, 044501 (2017).
- 44. M. Quick, A. L. Dobryakov, I. N. Ioffe, F. Berndt, R. Mahrwald, N. P. Ernsting, S. A. Kovalenko, J. Phys. Chem. B 122, 1049 (2018).
- 45. M. Quick, F. Berndt, A. L. Dobryakov, I. N. Ioffe, A. A. Granovsky, C. Knie, R. Mahrwald, D. Lenoir, N. P. Ernsting, S. A. Kovalenko, J. Phys. Chem. B, 118, 1389 (2014).
- 46. O. A. Krohn, M. Quick, I. N. Ioffe, O. N. Mazaleva, D. Lenoir, H. Detert, S. A. Kovalenko, J. Phys. Chem. B, 123, 4291 (2019).
- 47. M. L. Freile, S. Risso, A. Curaqueo, M. A. Zamora, R. D. Enriz, J. Mol. Struct. (THEOCEM) 731, 107 (2005).
- **48**. Ioffe, I. N.; Granovsky, A. A. Photoisomerization of Stilbene: The Detailed XMCQDPT2 Treatment,. J. Chem. Theory Comput. **9**, 4973 (2013).
- 49. X. Zheng, G. Zhai, W. Gao, Y. Lei, L. Yu, C. Zhu, Phys. Chem. Chem. Phys. 18, 8771 (2016).
- 50. N. Minezawa, M. S. Gordon, J. Phys. Chem. A, 115, 7901 (2011).
- 51. G. Mazur, M. Makowski, R. Wlodarczyk, Y. Aoki, Int. J. Quant. Chem. 111, 819 (2011).